JOURNAL OF AIRCRAFT
Vol. 37, No. 2, March–April 2000

Model Helicopter Rotor Aerodynamics and Acoustics As Measured in Two Anechoic Wind Tunnels

F. H. Schmitz*
University of Maryland, College Park, Maryland 20740
D. A. Boxwell†
U.S. Army Aviation and Missile Command, Moffett Field, California 94035
W. R. Splettstoesser‡ and K. J. Schultz‡
DLR, German Aerospace Research Center, D-38108 Braunschweig, Germany
S. Lewy§
ONERA, 92322 Chatillion, France
and
M. Caplot¶
Thompson–CSF, 78852 Elancourt, France

The qualities that are important for helicopter impulsive noise wind-tunnel testing are evaluated by comparing aerodynamic and acoustic data gathered on a single-scaled model main rotor that was tested in two open-jet wind anechoic wind tunnels of markedly different size: the CEPRA 19 tunnel in France and the DNW in The Netherlands. The rotor was instrumented with miniature blade-mounted pressure transducers and was tested on the same rotor test stand located within the flow of both open-jet wind tunnels. In-the-flow rotor acoustic signatures and selected on-blade dynamic pressure signatures are presented for each facility and discussed in relation to the differences in tunnel geometry, tunnel flow quality, and the aeroacoustic characteristics of each facility. This comparison shows that low background noise levels, a large in-the-flow anechoic measurement space, and low inflow turbulence to the rotor are necessary to yield high quality aerodynamic and acoustic data. The best match of acoustic data between the two facilities occurs when the tip-path plane of the rotor is chosen to match closely dynamic blade-surface-mounted pressures. Achieving a good match between scaled wind-tunnel acoustics and in-flight measurements are shown to be more difficult: Agreement is reasonably good at low advance ratios but marginal at higher advance ratios.

Nomenclature

A	= rotor disk area, πR^2
a_0	= speed of sound
C_T	= rotor thrust coefficient, $T/(\rho V^2 A)$
D	= diameter of the rotor, $2R$
M_{AT}	= rotor advancing tip Mach number, $M_H(1+\mu)$
M_H	= rotor hover tip Mach number, $(\Omega R)/a_0$
R	= rotor radius
r/D	= nondimensional distance between the microphone and the rotor hub
V	= forward velocity of the rotor
α_{TPP}	= tip-path plane angle of the rotor
$\Delta\alpha$	= peak-to-peak angle of attack wind-tunnel flow variations
μ	= advance ratio, $V/(\Omega R)$
ρ	= air density
ψ	= azimuth position of the rotor blade, measured from downstream

Received 31 August 1998; revision received 12 November 1999; accepted for publication 19 November 1999.

*Martin Professor of Rotorcraft Acoustics, Department of Aerospace Engineering. Associate Fellow AIAA.
†Research Scientist, Aeroflightdynamics Directorate.
‡Research Scientist, Technical Acoustics Department, Institute for Design Aerodynamics.
§Unit Head, Computational Fluid Dynamics and Aeroacoustics Department.
¶Technologies Coordinator, Radar and Countermeasures Division.

Introduction

MODEL-ROTOR aeroacoustic testing in wind tunnels by industry and government research organizations is now commonplace.[1–7] The impetus for this testing includes noise assessments to meet commercial noise regulations and military detectibility requirements, the use of new materials that allow the fabrication of accurately scaled rotor models, and the early evaluation of smart structures and active control technology to reduce rotorcraft noise radiation. It is important that rotorcraft manufacturers assess the acoustic characteristics of proposed new designs early in the development process. If the newly designed or modified rotorcraft is too noisy, it may not meet the requirements for flight in the commercial airspace or meet military acoustic detectablity requirements. Model-scale acoustic testing is proving to be an effective means of making these assessments.

In the past there have been two levels of aeroacoustic testing: one that has emphasized the evaluation of parametric design changes and one for quantification of fundamental noise-generation processes. There have been many successful attempts to assess the potential design changes on the radiated noise field (for example, see Refs. 4 and 5). In these experiments, the fidelity of the parametric results depended on the aerodynamic and acoustic properties of the testing facility and the degree to which the rotor testing was representative of full-scale flight. Wind tunnels with good aerodynamic flow properties and little reverberation in the frequency range of interest generally provided higher quality acoustic results. Similarly, those rotors with properly scaled aerodynamic and dynamic characteristics captured the important aerodynamic and acoustic phenomena and yielded more quantitative results. In this parametric testing approach, it was hoped that the phenomena being investigated were represented to adequate fidelity so that the effect of parametric design changes on the radiated noise of the actual helicopter rotor would be correct.

More quantitative aeroacoustic testing of model-scale rotors has been shown for certain types of helicopter noise. An in-flight, far-field method was used to gather a high-quality, full-scale acoustic database that was free from ground reflections.[8] The resulting data were used to compare the results of wind-tunnel tests of aerodynamically similar models. When relevant nondimensional parameters were held constant, excellent scaling of high-speed impulsive noise was demonstrated.[9] Good scaling at low advance ratios for blade-vortex interaction noise was also shown.[3] In neither case was it necessary to make corrections for Doppler shifts, ambient temperature, and wind effects. The impulsive noise phenomena of interest were quantitatively scaled.

Although always desirable, in many cases the more quantitative testing approach is not feasible. As a consequence, an important and interesting question arises: How much does the aerodynamic and acoustic properties of the facility itself influence the model-scale results? This paper addresses this question for rotorcraft impulsive noise by comparing rotor aeroacoustic data from tests on the same rotor tested in two different anechoic wind tunnels: the Centra d'Essais des Propulseurs (CEPr)—Office National d'Etudes et de Recherches Aérospatiales (ONERA)-19 (CEPRA-19) in France and the Deutsch-Niederlaendischer-Windkanal (DNW) in The Netherlands.

The test rotor was identical, and the tests were conducted in an identical manner in the two open-jet wind tunnels. The rotor was instrumented with many unsteady surface-pressure transducers to define, as completely as possible, the aerodynamics of the blade. In the following, an assessment of the aerodynamic and acoustic properties of both facilities is presented along with a brief description of the rotor and rotor stand. This is followed by a comparison of selected acoustic signatures and unsteady blade pressures taken in both wind tunnels. Both sets of scaled acoustic data are also compared with full-scale in-flight data to see how well the model-scale data replicates the impulsive events of full scale.

Facility Characteristics

General Features

Testing of the rotor model was first conducted in an anechoic wind tunnel located in France at the Centre d'Essais des Propulseurs near Paris. This facility, CEPRA 19, is of the open-circuit, open-test-section design and is one of the larger open-circuit anechoic wind tunnels in the world (Fig. 1a). A concrete test chamber, in the shape of one quadrant of a sphere with a 9 m radius, surrounds the open jet. The walls and floor are lined with acoustic wedges that are 1 m long, giving an acoustic cutoff frequency of about 200 Hz. Both the entrance and diffuser portions of the tunnel circuit are anechoically treated with acoustic baffles to protect the test chamber from exterior and tunnel-drive-system background noises.

The freejet of the CEPR-19 is 12 m long. A circular 3-m-diam nozzle was installed for these tests; theoretically it allows a maximum jet velocity of 60 m/s. The resulting flow is collected by a large, solid fiberglass collector and extracted by a centrifugal pump to the outside through an acoustic baffling system. For these tests, both the nozzle and collector were made of hard-surface fiberglass, and the nozzle lip was treated with 10 cm of serrated acoustic foam. An adjacent control room housed all measurement instrumentation and wind-tunnel and rotor drive controls. Table 1 lists the major geometric and flow characteristics of the freejet. Note that the level of transverse turbulence (1.1%) for CEPRA 19 in Table 1 is equivalent to rms angle-of-attack variations of about 0.6 deg in the jet. More detailed information about the CEPRA 19 facility is given in Refs. 10 and 11 and is summarized in Appendix A of Ref. 12. Note that since these rotor tests were run, modifications to the facility have been made that have improved the flow quality of the 3-m nozzle by an order of magnitude.

The DNW acoustic wind tunnel is a closed-return-type, subsonic atmospheric wind tunnel with three interchangeable, closed-test-section configurations and one open-jet aeroacoustic configuration; the latter was used for the model rotor tests. Figure 1b shows the arrangement of the various components of the DNW.

The open-jet configuration consists of a 6×8 m nozzle with a testing chamber surrounding the open jet that is 45 m long, 30 m wide, and 20 m high. The testing chamber walls are acoustically treated with 1.1-m wedges giving a cutoff frequency of about 80 Hz. The open-jet configuration was designed to obtain low background noise levels at flows up to 80 m/s. This was accomplished in the design of the facility by choosing a low-tip-speed fan (blade tip Mach number of 0.5) and by acoustically lining the turning vanes and the inner collector and transition walls. The major geometric and flow characteristics of the freejet are also summarized in Table 1 for comparison with the CEPRA 19 data. The comparative transverse turbulence level in the DNW of 0.1% (rms angle-of-attack variation of about 0.1 deg) indicates that the jet flow in the core of the jet is quite steady at frequencies above 0.2 Hz. More detailed information about the DNW facility characteristics are given in Refs. 13 and 14.

Rotor Installation Characteristics

The rotor used in both tests was a $\frac{1}{7}$-scale model of the AH-1/Operation Loads Survey (OLS) full-scale two-bladed rotor with pressure-instrumented blades that was used for aerodynamic and noise testing by NASA and Bell Helicopter (Refs. 3 and 15). The model rotor was instrumented with a number of miniature pressure

Table 1 Major geometric and flow characteristics of CEPRA 19 and DNW

Characteristics	CEPRA 19	DNW
Nozzle cross section	Circular, 3-m diam	Rectangular, 6×8 m
Free jet length, m	11.84	20.0
Mean flow velocity range, m/s	0–55	0–85
Axial turbulence level,[a] %	< 0.5	< 0.3
Transverse turbulence level,[a] %	< 1.1	< 0.1
α, peak-to-peak value	3.0	NA

[a]On centerline at 40 m/s.

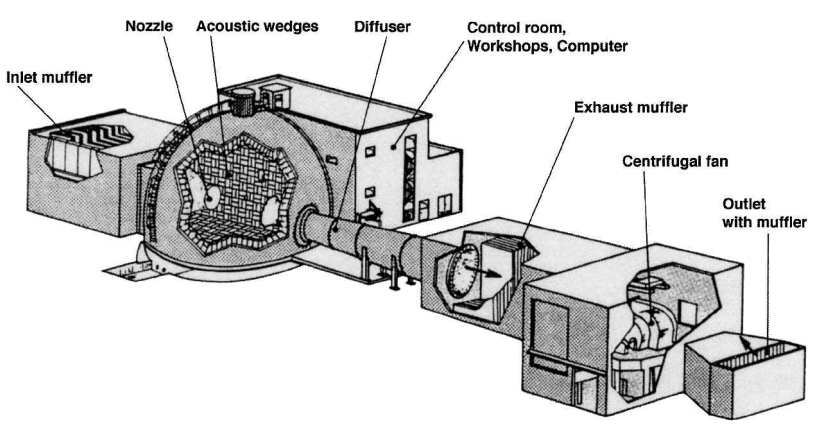

a) CEPRA 19 wind tunnel

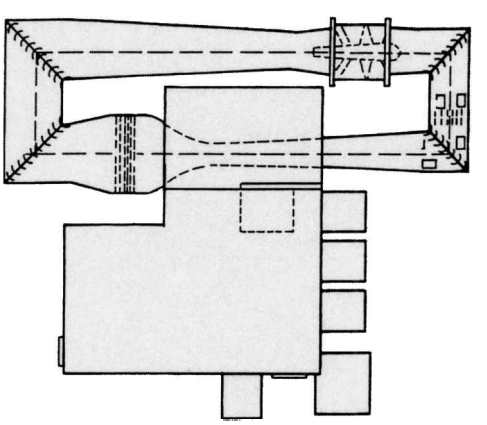

b) DNW wind-tunnel complex

Fig. 1 Two anechoic wind tunnels.

transducers to measure local surface-pressure distributions on the rotor blades. The rotor was mounted on a modular test stand secured to the floor of both facilities such that the upper part of the stand penetrated the open jet of both facilities. The upper part of the stand was similar for both test arrangements: It was aerodynamically fared and wrapped with acoustic treatment to avoid impulsive reflections. A more complete description of the rotor test stand is provided in Ref. 2 for the CEPRA 19 entry and in Ref. 3 for the DNW test. Figures 2a and 2b, taken from these references, illustrate the rotor installation in the open jet of each facility. For each installation, microphones were distributed around the rotor: both within the freejet and outside of the open-jet core flow. Several of the in-flow microphones were located at the same nondimensional positions in each facility.

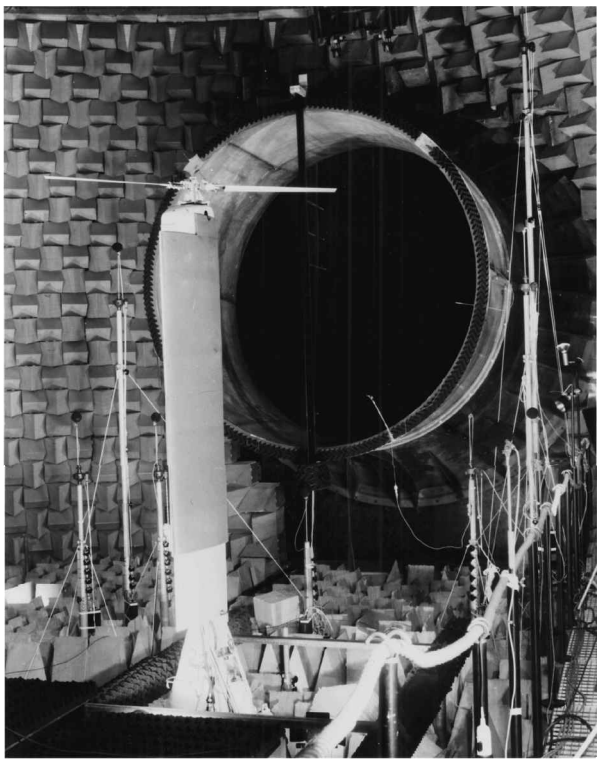

a) Installed in CEPRA 19

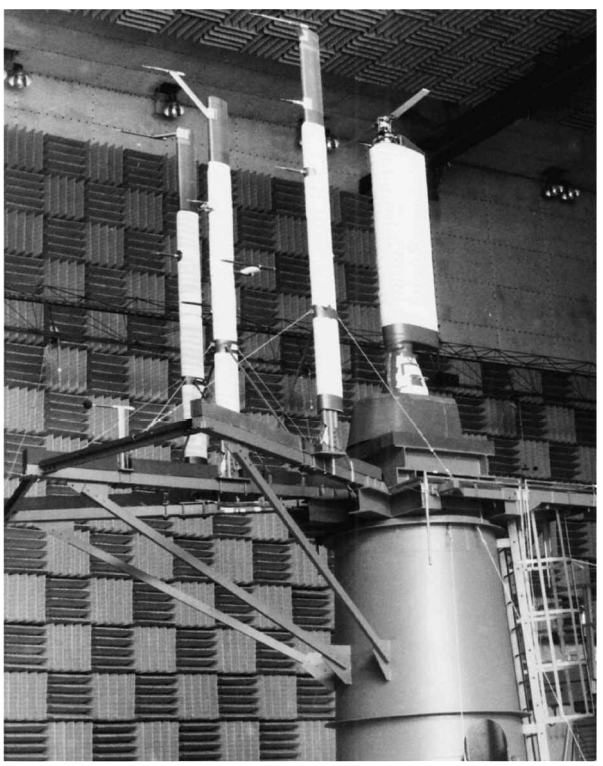

b) Installed in the DNW open test section

Fig. 2 One-seventh-scale model OLS rotor and test stand.

Inherent in wind-tunnel testing of model helicopter rotors is a large variety of possible operating conditions, one of which is the variation of the rotor's tip-path-plane angle with respect to the freestream flow. For both tunnels, it was assumed the similar rotor installations (both tests used the same rotor, rotor hub, and test stand) did not alter the airflow qualities of the test. Open-jet wall corrections were estimated before testing,[2,16] but because of prediction uncertainties, they were only used to guide the selection of planned test conditions. Instead, parametric sweeps were conducted in both tunnels to map out critical testing parameters carefully, for instance, a sweep of the rotor tip-path-plane angle, which is known to be sensitive to open-jet boundary effects. In this manner, blade–vortex interaction (BVI) geometry critical to rotor acoustics would not be missed in either tunnel installation. (The effect of this will be seen in data presented in a later section.)

The acoustic characteristics of each facility, however, were not assumed to be those of previously published tunnel surveys. The effect of rotor installation, for example, struts and fairings, on each tunnel's acoustic environment was investigated before testing was begun. Two methods were used: 1) background tunnel noise measurement (no rotor running) and 2) impulsive calibrations.

Background Noise

Background noise was measured on all microphones, both in the flow and out of the flow for both tunnels. Results are presented for two microphone locations 1.5 diameters directly ahead of the rotor in a hub-centered coordinate system: one in a plane normal to the vertical and passing through the rotor hub (in-plane) and one down 30 deg from that plane. The out-of-flow microphones are not used in this paper. Treating the unsteady effects of the open-jet shear layer on radiated rotorcraft acoustics is beyond the scope of this work. Background noise measurements were analyzed in 40-Hz narrow bands from dc to 10 kHz with no high-pass filtering.

The measured levels for the in-plane microphone, as a function of tunnel velocity, are illustrated in Fig. 3a for CEPRA 19 and in Fig. 3b for the DNW [sound pressure level (SPL) in decibel RE 2×10^{-5} Pa]. Both tunnels exhibit in-the-flow background noise levels that are low enough to permit the measurement of model-rotor impulsive noise signatures. The inflow noise levels for both tunnels are characterized by higher spectrum levels at frequencies below 100 Hz and by a gradual decay in level toward the higher frequencies, where levels are typically dominated by wind-induced noise from the nose cone on the microphone. Above 35 m/s, the CEPRA 19 spectra show generally higher noise levels above 100 Hz. Part of this increase in level occurs around discrete frequencies, probably a result of vortex shedding from microphone struts or other pieces of the rotor installation structure. The CEPRA 19 background noise at 50 m/s exhibits a gradual increase in level with frequency that is thought to result from broadband loads on the microphone nose cone and support strut. These loads are likely induced by the larger unsteady angle-of-attack variations in the CEPRA 19 flow and raise the background threshold by approximately 10 dB at frequencies above 5 kHz (15 dB above the DNW background noise). The inset in Figs. 3a and 3b shows more clearly the low-frequency background spectrum levels near the rotor fundamental blade-passage frequency of about 80 Hz. Here the background levels can be nearly the same order of magnitude as the expected rotor noise levels, but averaging techniques can be used to extract the lower rotor noise harmonics from the measured signal.

Background noise for the inflow microphone located 30 deg below the in-plane position is shown in Figs. 4a and 4b for CEPRA 19 and DNW, respectively. The evidence of shedding noise in CEPRA 19 has diminished at this location, and the DNW levels at 80 m/s have increased slightly, probably a result of shear-layer proximity.

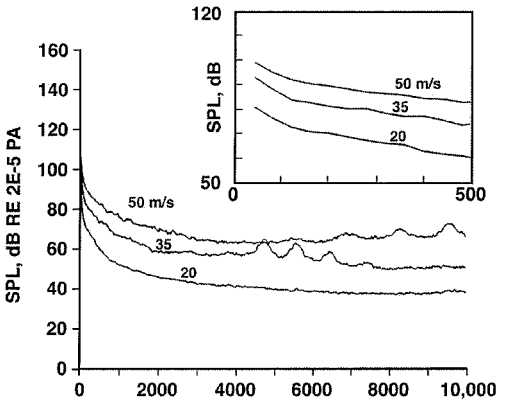

a) CEPRA 19

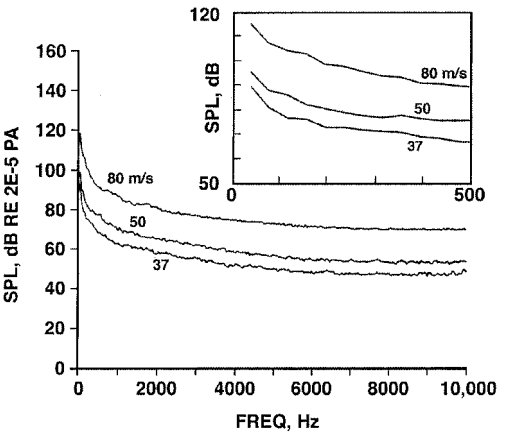

b) DNW

Fig. 3 In-flow background noise vs tunnel velocity for the forward in-plane microphone position.

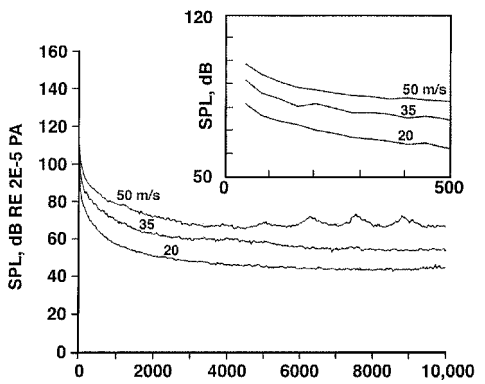

a) CEPRA 19

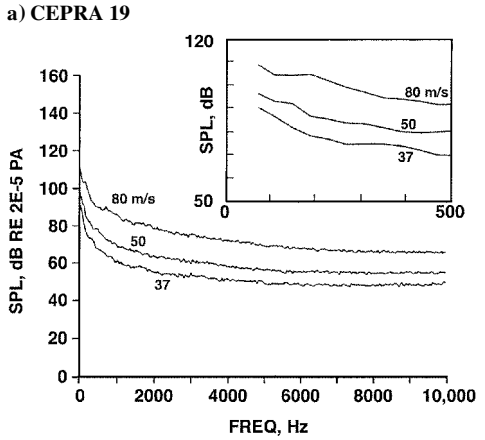

b) DNW

Fig. 4 In-flow background noise vs tunnel velocity for the microphone 30 deg down from the in-plane microphone position.

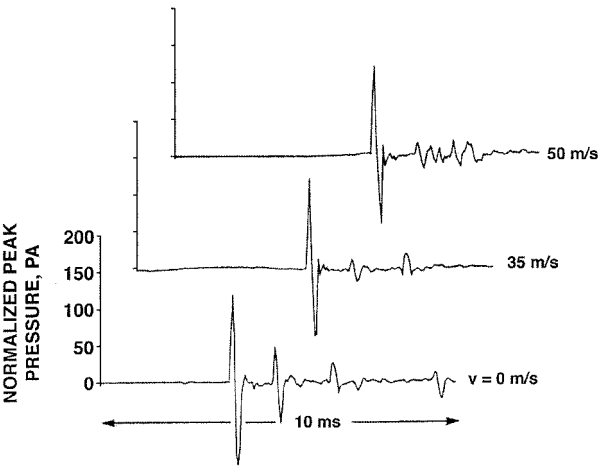

a) CEPRA 19

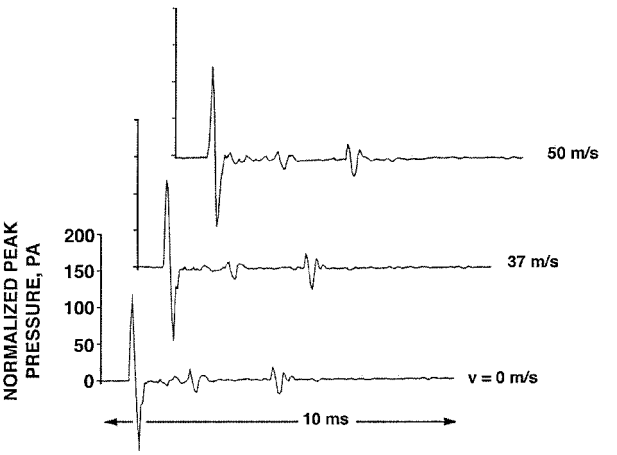

b) DNW

Fig. 5 Wind-tunnel impulse calibration for several tunnel velocities for the straight-ahead in-plane microphone.

Impulse Calibrations

The second method for assessing the anechoic properties of both wind tunnels used impulsive devices (small explosive charges mounted in the plane of the rotor disk and fired electrically) to determine acoustic reflections. These initial reflection tests revealed unwanted acoustic reflections from the 3-m nozzle lip and the rotor stand in CEPRA 19 and from the microphone support struts in the DNW. Prior to the acquisition of acoustic data, the rotor test stand was covered with acoustic treatment in CEPRA 19. Absorptive material was also added to the microphone support structure in the DNW for the purpose of reducing reflections by at least 10 dB.

Figures 5 and 6 show the time histories of the reflection tests for the in-plane and 30-deg-down microphone positions. The time histories for the in-plane microphones (Figs. 5a and 5b) in both tunnels indicated that the reflections were significantly reduced after acoustic treatment,[12] with the DNW almost approximating free-field conditions. Unfortunately, and because of scaling constraints, the CEPRA 19 microphone located 30 deg below the in-plane microphone (Figs. 6a and 6b) was positioned close to the acoustically untreated nozzle and resulted in a reflection that was stronger than desired. The problem became more severe with flow when multiple nozzle and/or shear-layer reflections were observed to follow the initial impulse. The effect of these reflections is to distort both the time histories and the power spectra of the measured rotor noise.

Rotor Acoustic Comparisons

Figures 7–9 present a direct comparison of the model-scale OLS blade acoustic signatures as measured in the two facilities along with the corresponding full-scale 540-rotor (OLS) acoustic signatures as measured in-flight. The left-hand sides of Figs. 7–9 illustrate the

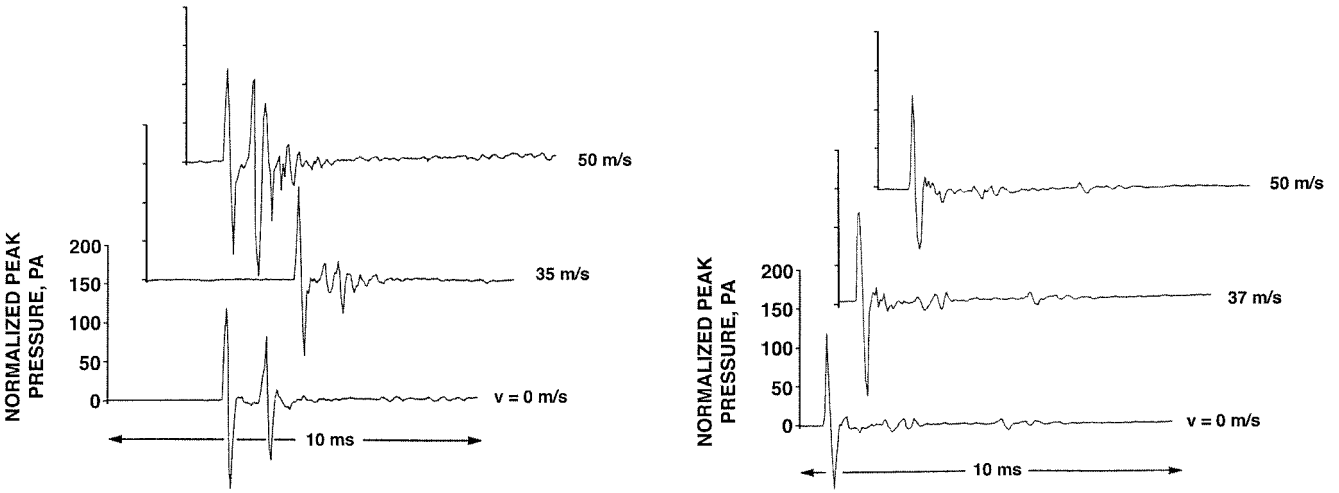

a) CEPRA 19 b) DNW

Fig. 6 Wind-tunnel impulse calibration for several tunnel velocities for the straight-ahead 30-deg-down microphone position.

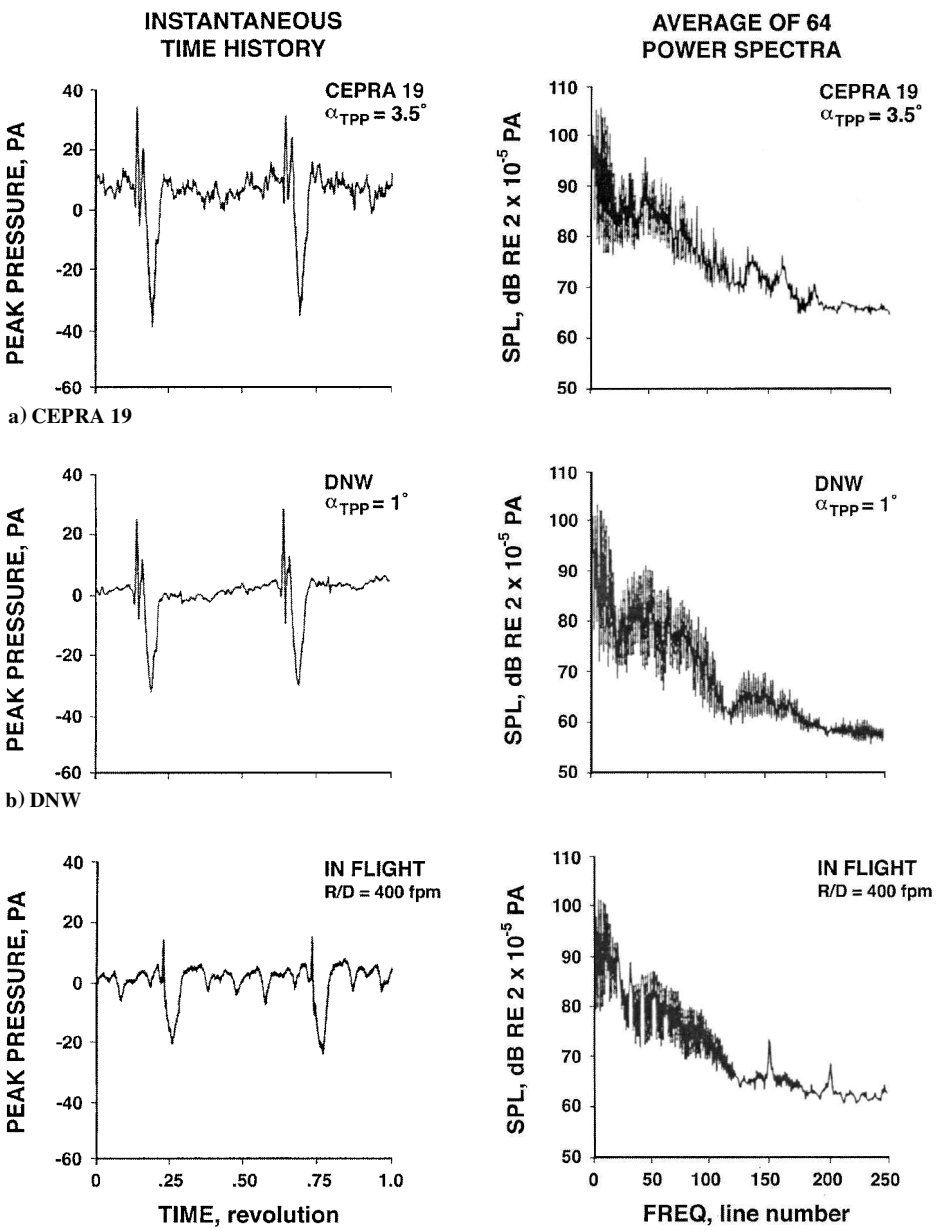

a) CEPRA 19

b) DNW

c) Full-scale flight test

Fig. 7 In-plane rotor acoustic comparisons; $\mu = 0.164$, $M_{AT} = 0.772$, and $C_T = 0.0054$.

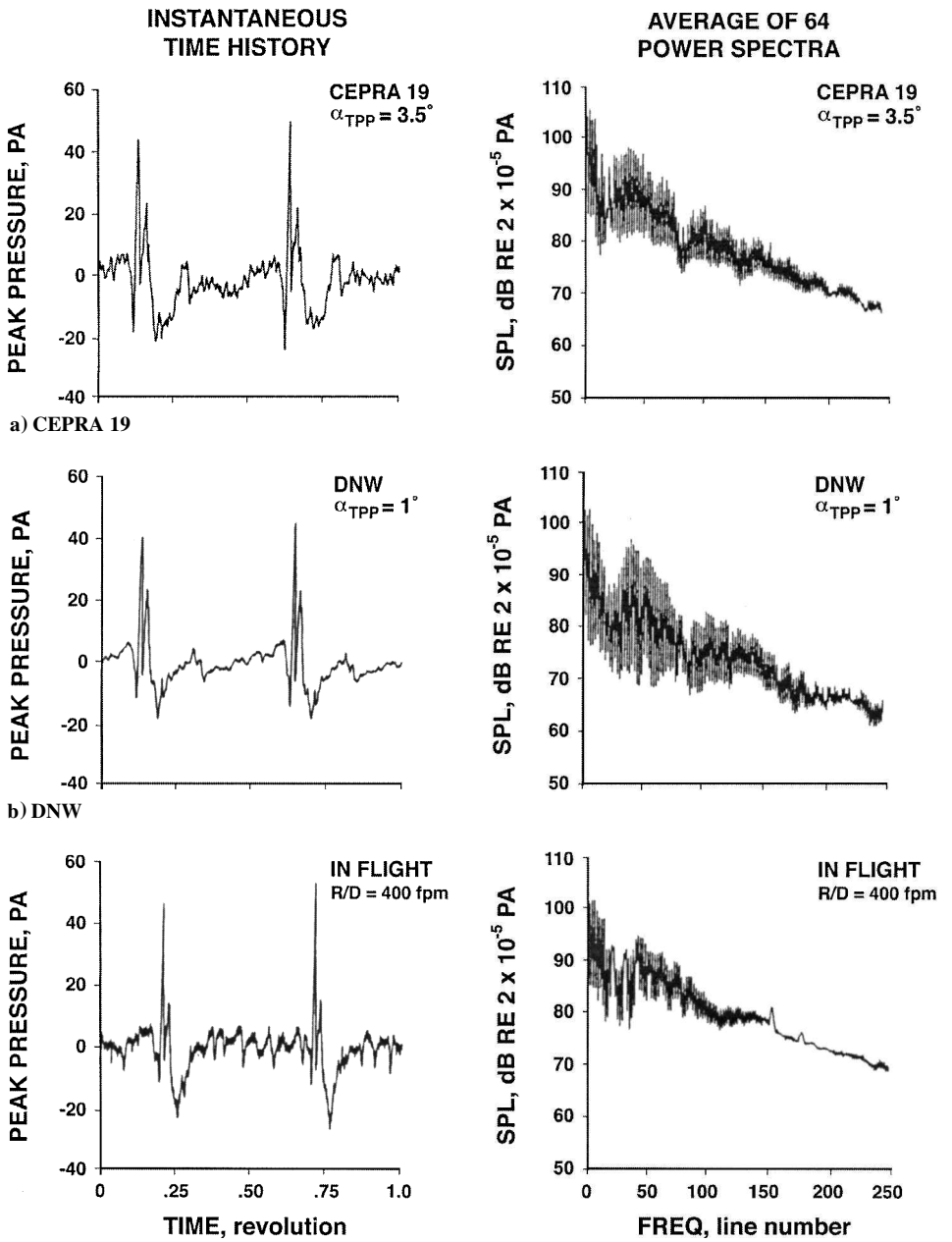

Fig. 8 Acoustic comparisons (30 deg down from in-plane microphone position); $\mu = 0.164$, $M_{AT} = 0.772$, and $C_T = 0.0054$.

instantaneous time history over one revolution whereas the right-hand sides of Figs. 7–9 illustrate the average of 64 power spectra of successive time histories. The start times (time ~ 0 or 1.0) for both model-scale and the full-scale times histories are somewhat arbitrary. The model-scale start times are similar because the geometry of the microphones and the test conditions that are compared were the same in both facilities and the start time was referenced to the downstream rotor blade position. The full-scale start times are arbitrary. The power spectra data are displayed over a harmonic frequency axis, where each line unit is a measure of rotor rotational rate (about 40 Hz for model scale). For this two-bladed rotor, every other line in the spectrum is exactly a rotor harmonic of blade-passage frequency. The 250-line frequency responses in Figs. 7–9, therefore, correspond to about 10 kHz in model scale.

Figure 7 presents acoustic comparisons for an in-plane microphone at a nominal advance ratio of 0.164 and a thrust coefficient of 0.0054. As will be explained in a following section, blade pressures were used to determine comparable rotor flight conditions (performance states) in each facility. Figure 7a presents in-plane CEPRA 19 time history acoustic data for a rotor tip-path-plane angle of 3.5 deg; Fig. 7b presents DNW data at 1 deg, indicating a 2.5-deg jet angularity difference between facilities at this rotor advance ratio and thrust coefficient. This difference in tip-path-plane angle is most likely due to the different wind-tunnel wall effects of both facilities. The full-scale results in Fig. 7c were measured during a 400-ft/min rate of descent, which theoretically corresponds to a tip-path-plane angle of 2 deg (Ref. 3).

The time histories, when matched in this manner, show good overall similarity between model-scale results, especially when one considers the order of magnitude difference in unsteady flow angles that existed between facilities. The key events of high-speed impulsive (HSI) thickness noise (negative pulse at time ~ 0.22 and 0.77) and BVI noise (positive peaks at time ~ 0.2 and 0.75) have been captured. The time histories in the DNW are, however, more distinct than those in CEPRA 19. The higher background noise and the general unsteadiness of the rotor flow cause the time history of the CEPRA 19 data to be choppier. The frequency-domain results follow these same trends with the DNW averaged spectra having

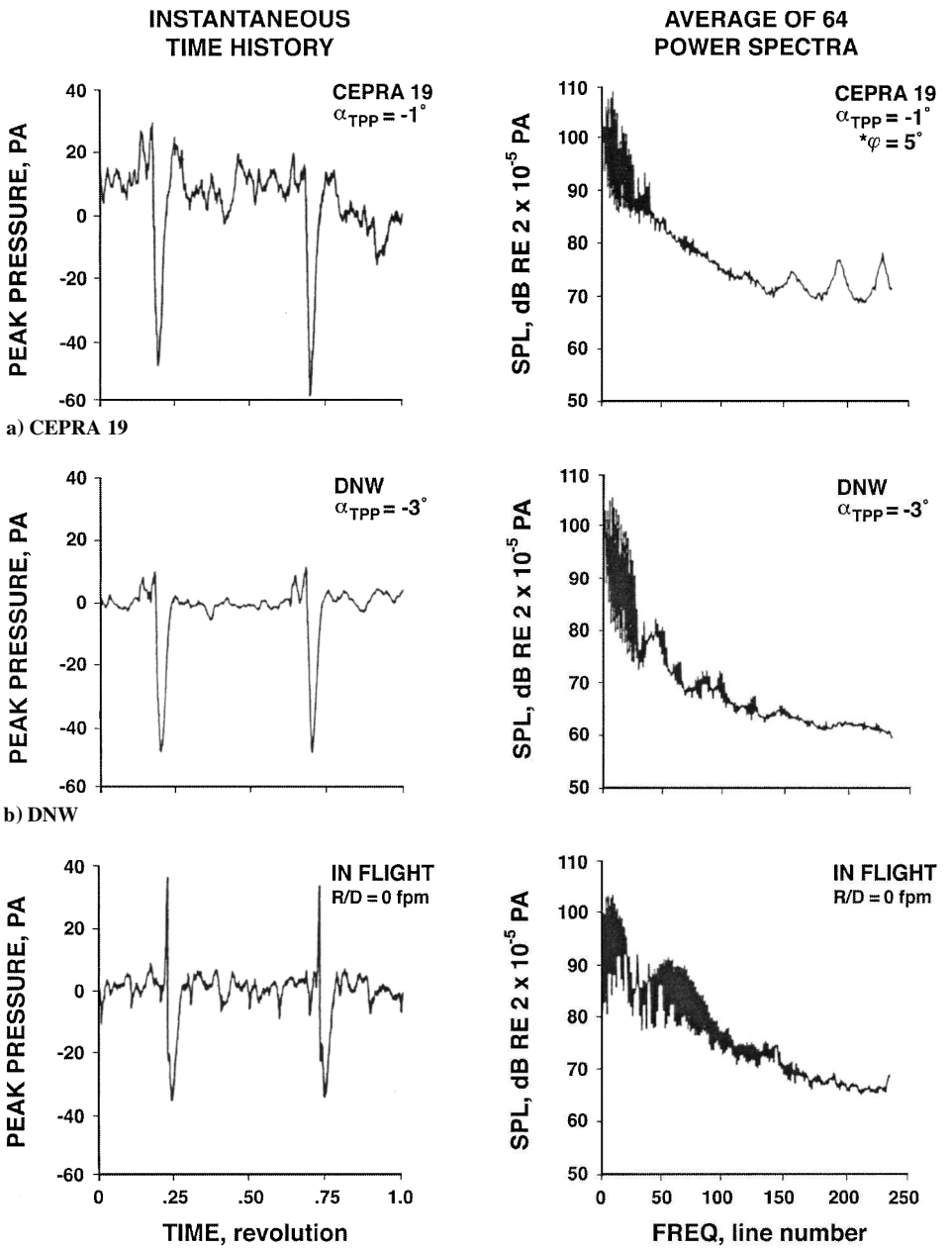

Fig. 9 In-plane rotor acoustic comparisons; $\mu = 0.224$, $M_{AT} = 0.807$, and $C_T = 0.0054$.

a better signal-to-noise ratio than CEPRA 19. The location of the in-plane microphone within the hard-walled nozzle of CEPRA 19 is probably responsible for the small differences in the spectral shapes at low frequencies, whereas differences at higher frequencies are thought to be related to the larger angle-of-attack inflow variations of CEPRA 19. Note that the average power spectrum of the flight-test data retains the tail-rotor-related frequencies in the full-scale measurements. These tail-rotor peaks/harmonics can be removed from the data by averaging the data as shown in Ref. 8. This averaging procedure allows a more direct comparison of model- and full-scale results.

The comparison between flight-test and wind-tunnel acoustic data is not quite as good. Although the HSI noise pulse shapes match quite well, the comparison of high-speed thickness noise (time ~ 0.22 and 0.77) shows the flight amplitude of the thickness noise pulse is lower (by about 25%) than the DNW wind-tunnel measurements at this in-plane microphone position. Differences in BVI noise (time ~ 0.2 and 0.75) are also noted. In general, the wind-tunnel data appear larger in amplitude for this in-plane microphone position and have somewhat different BVI time histories. There are several possible reasons for this lack of quantitative correlation between flight-test and wind-tunnel acoustic data. Because the flight condition of the rotorcraft was not chosen by comparing flight blade pressure data with wind tunnel blade pressure data as it was with the CEPRA 19 and DNW data, it is possible that the operating aerodynamic states of the rotors were not exactly the same. The fidelity of the wind-tunnel wall corrections as well as facility reverberation characteristics also can influence these comparisons.

Figure 8 shows acoustic data taken at the same testing condition for a microphone position 30 deg below the in-plane microphone. At this measurement location, the BVI acoustic signature (time ~ 0.2 and 0.7) is stronger in both model- and full-scale results; however, the CEPRA 19 data show the effect of tunnel-nozzle contamination, mentioned earlier in the discussion of impulse calibrations. The rotor signature in the CEPRA 19 depicts a wider thickness noise component (time ~ 0.25 and 0.75), probably due to nozzle reflections and/or shear-layer distortions. This is also indicated by the higher level, low-frequency content in the CEPRA 19 spectral

plots. Similar to the in-plane position, higher frequency spectral differences between the data taken in the two wind tunnels are noted at the 30-deg-down measurement position. The DNW data are again more distinct than the CEPRA 19 data and, for this microphone position, scale with the full-scale data quite well.

Figure 9 presents results for the in-plane microphone at an advance ratio of 0.224, a condition known to produce HSI noise (time ~ 0.25 and 0.75). The in-plane microphone position is chosen for comparison because it is known that maximum HSI noise is in this direction. For this higher advance ratio, a tip-path-plane correction of 2 deg between facilities was estimated. In-plane HSI noise (time ~ 0.25 and 0.75) wind-tunnel pulse shapes match quite well at this in-plane microphone position, but the amplitude of the CEPRA 19 measurements are slightly larger than the DNW measurements, which are also larger than the full-scale measurements by about 25%. Differences between model-scale and full-scale peak pressure levels and waveforms of the BVI noise (time ~ 0.2 and 0.7) become more evident at this higher speed. The CEPRA 19 data are the least well defined, but neither model-scale test closely replicates the full-scale results. These discrepancies can also be seen in the power spectra data (right-hand side of Fig. 9). In the CEPRA 19 tunnel, the signal-to-noise ratio of the acoustic signature is generally lower, and the spectral shapes are different when compared with DNW data for the reasons cited earlier. The DNW power spectra data are better defined than CEPRA 19 data, but exhibit a marked difference when compared with full-scale data.

As mentioned earlier, the in-flight data was not matched using the blade surface pressures to either wind-tunnel test because no full-scale blade pressure data are available that could be used to match the rotor aerodynamic states. This may have resulted in a slight miss match in the rotor aerodynamics between flight test and wind tunnel and is a possible explanation for the discrepancies at this high-speed helicopter flight condition. Differences in actual measurement angles and unsteady flow angularities are two additional possible explanations for this lack of signature correlation.

Rotor Aerodynamic Comparisons

The scale-model AH-1/OLS rotor was instrumented with 50 miniature pressure transducers: 32 absolute, flush-mounted Kulite transducers on one of the blades and 18 differential pressure transducers on the second blade. The absolute transducer locations were chosen to match some of the radial and chordwise transducer

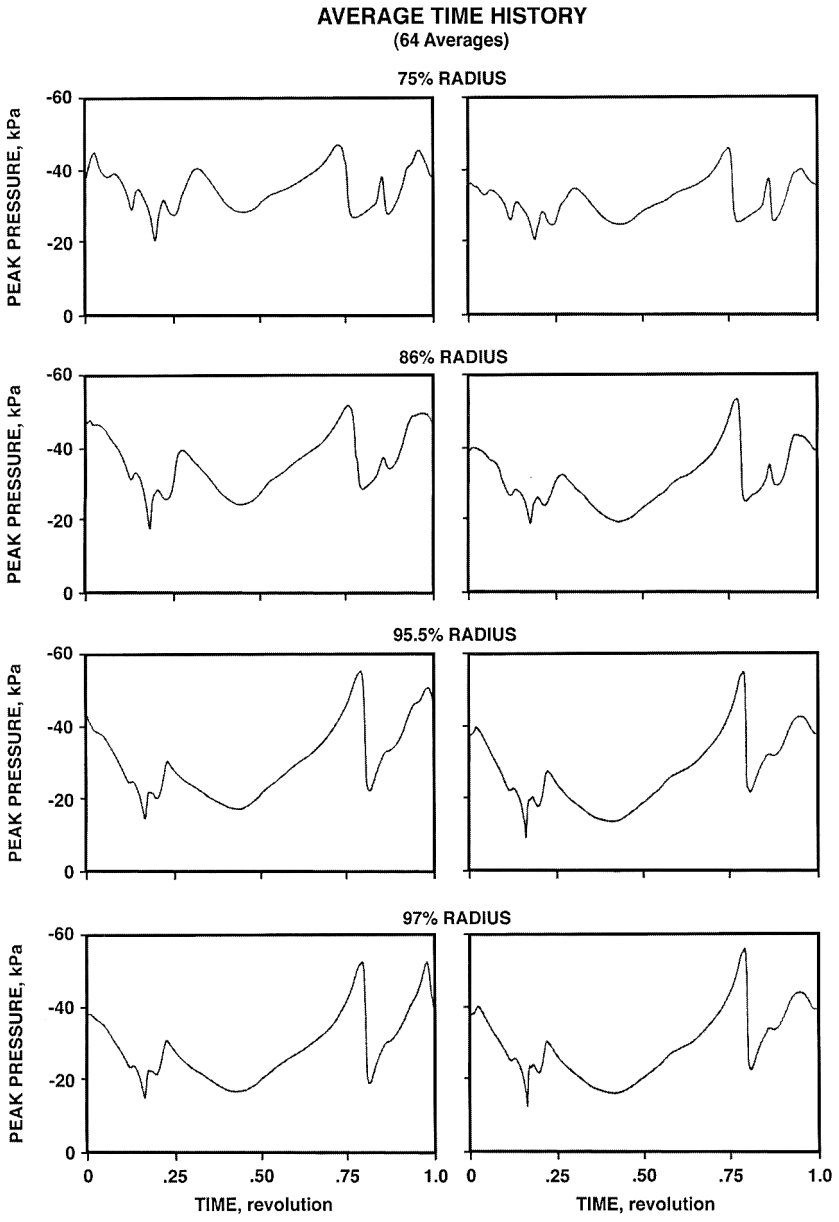

Fig. 10 Upper surface model rotor blade dynamic pressure time histories for several radial positions; $\mu = 0.164$, $M_{AT} = 0.772$, and $C_T = 0.0054$.

positions in the full-scale NASA OLS tests.[15] The geometrical characteristics of the model blades and the model-scale transducer locations are given in Ref. 9.

As already discussed, the flow aerodynamics of each wind tunnel can alter the true operating state of the rotor. To account for these changes, flow corrections (wall corrections) for each facility are usually predicted and applied to the measured performance of the rotor. For example, a simple theoretical wall correction model was used in Ref. 2 to indicate that a 1.5-deg correction was appropriate to match CEPRA 19 model data with full-scale data. Because the rotor blades were instrumented with pressure transducers, a more straightforward method of matching operating conditions was chosen. Measured blade-pressure time histories were simply compared over a range of operating conditions to find the condition in each facility that made the aerodynamics on the blade most similar.

One flight condition, at an advance ratio of 0.164, is chosen to illustrate the comparison of blade pressures measured in the CEPRA 19 and DNW anechoic wind tunnels. For this advance ratio and at a constant thrust coefficient of 0.0054, a parametric sweep of tip-path-plane angle was performed in each facility. These rotor sweep angles (from −5 to +7 deg in the DNW and from 0 to +5 deg in CEPRA 19) placed the rotor in a series of flight conditions (descents) known to produce BVI. The measured blade pressures and resulting air loads during this parametric sweep of rotor tip-path-plane angles were extensively analyzed and compared. This comparison clearly showed that to match the aerodynamic state of the rotor by attempting to match blade pressures/loads, an angular tip-path-plane difference of about 2.5 deg was required between facilities at this flight condition. The comparison also showed that using blade pressures to correct for influences of wind-tunnel wall effects is a more sensitive method than trying to match acoustic time histories for the same purpose. The 2.5-deg correction was used in the following comparisons.

Figure 10 presents averaged upper-surface (leading edge 3% chord), blade-pressure time histories at four blade radial stations after this angle-of-attack correction procedure had been applied. The data are shown for one rotor revolution with time = 0 representing the downstream position of the blade. Figures 10a and 10b show the CEPRA 19 and DNW results, respectively. The data show that although the measured blade pressures are matched quite well on an average basis, differences still remain. In particular, it was impossible to obtain a perfect time history match for both the inboard and outboard radial pressure transducers. At the more inboard radial stations at the position of advancing BVI (time ~ 0.2), the CEPRA 19 impulses are slightly larger than the DNW pulses. At the outboard radial stations, the reverse is true. This implies that the wind-tunnel facility distortions on the flow are not entirely correctable by simple matching of blade pressures/loads. There are other facility factors besides tip-path-plane angle that influence the comparison.

There are also some notable differences in the sharpness of the advancing BVI pulse (time ~ 0.2) at the outboard radial stations as seen in Fig. 10. The DNW blade pressure data have very sharp BVI time histories and apparently higher signal-to-noise ratios than the CEPRA 19 data. It is most likely that the higher transverse turbulence levels of the CEPRA 19 tunnel have had an adverse influence on the CEPRA 19 measured blade pressures, smoothing out the pulse time histories in most cases. Differences in blade-pressure time histories are also notable at the outer radial stations (0.97 radius) at the downstream positions of the rotor (time ~ 0.95) as seen in Fig. 10. Because the rotor tip-path-plane angle is 2.5 deg more positive (flapped back) in the CEPRA 19 tunnel than in the DNW, it is closer to the wake of the strut fairing and, therefore, sees a more pronounced effect.

Figure 11 compares the upper- and lower-surface leading-edge (3% chord) blade pressures at nearly the same radial station (within 1% of the 96% blade radius) in the time (left-hand side of Fig. 11) and frequency (right-hand side of Fig. 11) domains. The instantaneous time histories for the CEPRA 19 and DNW have been chosen to be comparable in level to the average signal over the sampling period.[10] As shown in the left-hand side of Fig. 11, the DNW blade surface-pressure data near the advancing BVI locations (time ~ 0.2),

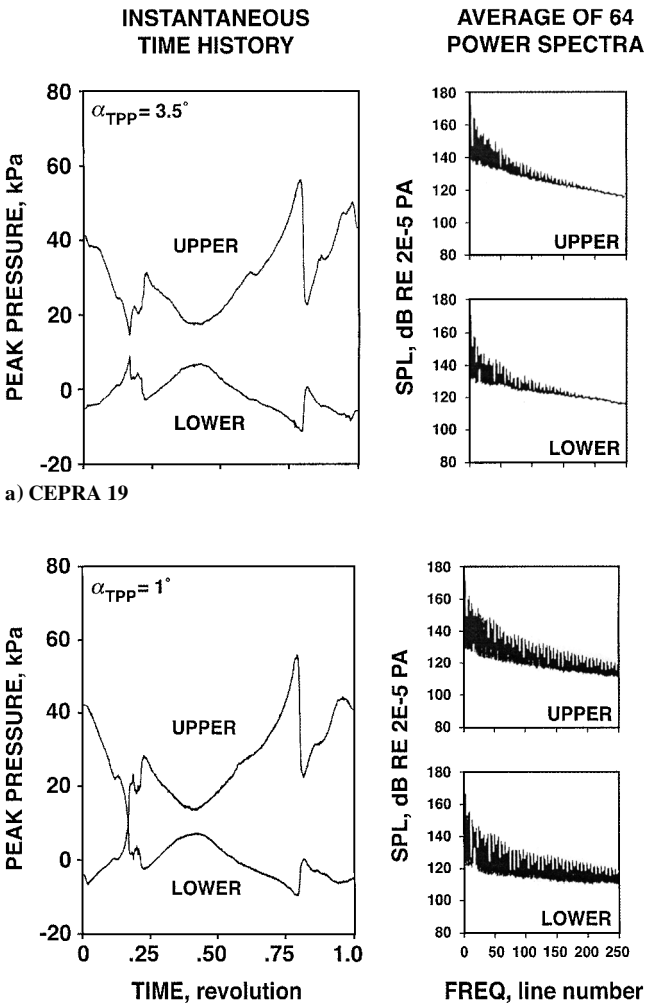

Fig. 11 Upper and lower surface model rotor blade dynamic pressure time histories and corresponding average power spectra for one radial position (~ 0.96 *R*); $\mu = 0.164$, $M_{AT} = 0.772$, and $C_T = 0.0054$.

are sharper and are indicative of a more distinct impulsive event than similar data taken in the CEPRA 19 wind tunnel. This same effect is seen in the right-hand side of Fig. 11 as a slower harmonic rolloff in the corresponding average power spectrum of the DNW data when compared with CEPRA 19 data. These power spectra are computed on two-revolution time histories and averaged over 64 cycles. This gives a frequency resolution and response (250 lines) of about 20 Hz and 5 kHz, respectively. The periodic nature of BVI is also evident in the averaged-power spectra as discrete frequency harmonics. Higher harmonics of BVI are more clearly defined in the DNW than in the CEPRA 19 blade surface-pressure data. This reinforces the observation that the periodic events that were measured in the DNW tunnel were more distinct than those measured in CEPRA 19 under the same simulated flight condition (performance state).

Conclusions

It has been shown that both the CEPRA 19 and DNW facilities exhibit in-the-flow background noise levels low enough to permit the accurate measurement of model-scale radiated impulsive acoustic signatures. In the DNW, the rotor impulsive noise signatures were above inflow background noise levels at flow velocities up to 80 m/s. The CEPRA 19 background noise levels were higher than the DNW (~ 10–12 dB) at low and high frequencies, probably due to the higher turbulence levels in the CEPRA 19 facility.

Having a large anechoic in-the-flow testing space is important for quantitative acoustic measurements. For the size of rotor that was tested (2 m diam), the DNW in its 6 × 8 m open-jet nozzle

configuration allowed scaled placement of inflow microphones farther from the nozzle structure and from the freejet shear layer than in the CEPRA 19 with its 3-m nozzle. Impulsive calibrations indicated that the 3-m nozzle of the CEPRA 19 would contaminate the microphone data at the 30 deg below the in-plane microphone position where strong BVI impulsive noise signatures are radiated. These effects were observed in the CEPRA 19 acoustic data in both the time and frequency domains.

Higher rms transverse turbulence levels (an order of magnitude larger) in CEPRA 19, as compared with the DNW, affected the measured acoustic data. Although the spectral shape in the lower frequency harmonics (100–2000 Hz) was generally the same in both facilities, differences in specific harmonic levels of up to 10 dB were noted. This caused the BVI acoustic and onblade pressure time history measurements to be more distinct in the DNW facility than those measured in CEPRA 19.

Matching the performance state of the rotor between facilities was greatly facilitated by the use of onblade pressure transducers. Blade pressure measurements taken during rotor-tip-path plane parametric sweeps indicated that a 2.5-deg tip-path-plane angular flow difference (flow correction) existed between the two facilities at an advance ratio of 0.164 and a thrust coefficient of 0.0054. This was in contrast to a theoretically estimated correction of 1.5 deg. When the experimental correction was accounted for, averaged-measured blade pressures were more similar in character in both facilities.

HSI acoustic waveforms and power spectra at in-plane microphone measurements ahead of the helicopter were quite similar for both facilities. Some small differences in levels were observed. Comparison of HSI wind-tunnel acoustic data with flight acoustic data revealed good pulse shape correlation but some discrepancies in amplitude. Model-scale acoustic data overpredicted the levels of full-scale HSI noise (by about 25%) at the in-plane microphone position.

BVI acoustic waveforms and power spectra matched quite well between the CEPRA 19 and DNW wind tunnels, but did not match as well when compared with full-scale BVI data. That the full-scale rotor performance state was estimated and not determined by using measured flight dynamic pressure measurements (which are not available) is thought to be a major reason for this lack of correlation. Future programs that attempt to compare flight and wind-tunnel acoustics should match rotor performance states by attempting to match measured blade surface dynamic pressures.

In summary, it has been shown that it is generally possible to make quantitative and consistent rotor acoustic measurements in different open-jet, anechoic wind tunnels that contain the important features of impulsive noise. Low background noise levels, a large anechoic inflow testing space, low flow turbulence of the jet, and careful matching of the aerodynamic state of the rotor all contribute to a high-quality test that can replicate many features of full-scale rotor impulsive noise data.

References

[1]Sternfeld, H., and Schaeffer, E. G., "The Role of Wind Tunnel Models in Helicopter Noise Research," *Proceedings of the 42nd Annual National Forum of the American Helicopter Society*, American Helicopter Society, Alexandria, VA, 1986, pp. 513–524.

[2]Schmitz, F. H., Boxwell, D. A., Lewy, S., and Dahan, C., "Model- to Full-Scale Comparisons of Helicopter Blade–Vortex Interaction Noise," *Journal of the American Helicopter Society*, Vol. 29, No. 2, 1984, pp. 16–25.

[3]Splettstoesser, W. R., Schultz, K. J., Boxwell, D. A., and Schmitz, F. H., "Helicopter Model Rotor Blade–Vortex Interaction Impulsive Noise: Scalability and Parametric Variations," NASA TM-86007, Aug. 1984; also 10th European Rotorcraft Forum, Paper 18, Aug. 1984.

[4]Hoad, D. R., "Helicopter Model Scale Results of Blade–Vortex Interaction Noise as Affected by Tip Modification," *Proceedings of the 36th Annual National Forum of the American Helicopter Society*, American Helicopter Society, Alexandria, VA, Preprint 80-62, 1980.

[5]Conner, D. A., and Hoad, D. R., "Helicopter Model Scale Results of Blade–Vortex Interaction Impulsive Noise as Affected by Blade Planform," 38th Annual Forum of the American Helicopter Society, May 1982, pp. 528–537.

[6]Tung, C., Kube, R., Brooks, T. F., and Rahier, G., "Prediction and Measurement of Blade–Vortex Interaction," *Journal of Aircraft*, Vol. 35, No. 2, 1998, pp. 260–266; also AIAA Paper 95-021, 1995.

[7]Gallman, J. M., Schultz, K. J., Speigel, P., and Burley, C. L., "Effect of Wake Structure on Blade–Vortex Interaction Phenomena: Acoustic Prediction and Validation," *Journal of Aircraft*, Vol. 35, No. 2, 1998, pp. 267–273; also AIAA Paper 95-022, 1995.

[8]Schmitz, F. H., and Boxwell, D. A., "In-Flight Far-Field Measurement of Helicopter Impulsive Noise," *Journal of the American Helicopter Society*, Vol. 21, No. 4, 1976, pp. 2–16.

[9]Boxwell, D. A., Schmitz, F. H., Splettstoesser, W. R., and Schultz, K. J., "Helicopter Rotor High-Speed Impulsive Noise: Measured Acoustics and Blade Pressures," NASA TM-85850, 1983.

[10]Bongrand, J., Julienne, A., and Perulli, M., "Simulation of the Effects of Forward Velocity on Jet Noise in an Open Circuit Wind Tunnel," ONERA Preprint 1978-6E; also Workshop on the Effects of Forward Velocity on Jet Noise, 1976.

[11]Rebuffet, P., and Guedel, A., "Tests on an 8/100-Scale Model for the Definition of the Convergent Collector of CEPRA 19 (Anechoic Open Jet Wind Tunnel)," AIAA Paper 81-1989, 1981.

[12]Boxwell, D. A., Schmitz, F. H., Splettstoesser, W. R., Schultz, K. J., Lewy, S., and Caplot, M., "A Comparison of the Acoustic and Aerodynamic Measurements of a Model Rotor Tested in Two Anechoic Wind Tunnels," 12th European Rotorcraft Forum, Paper 38, 22–25 Sept. 1986.

[13]Michel, U., and Froebel, E., "Velocity Fluctuations in the German–Dutch Wind Tunnel Relevant to Rotor Noise Measurements," DLR, German Aerospace Research Center, DFVLR IB-22216-85/B1, Braunschweig, Germany, Dec. 1985.

[14]Van Ditschuizen, J. C. A., Courage, G. D., Ross, R., and Schultz, K. J., "Acoustic Capabilities of the German–Dutch Wind Tunnel, DNW," AIAA Paper 83-0146, 1983.

[15]Cox, C. R., "Helicopter Rotor Aerodynamic and Aeroacoustic Environments," AIAA Paper 77-1338, Oct. 1997.

[16]Heyson, H. H., "Rapid Estimation of Wind Tunnel Corrections with Application to Wind Tunnel and Model Design," NASA TN D-6416, 1971.